


## Article

# Monitoring Land Use Changes and Their Future Prospects Using GIS and ANN-CA for Perak River Basin, Malaysia

Muhammad Talha Zeshan <sup>\*</sup>, Muhammad Raza Ul Mustafa <sup>\*</sup>  and Mohammed Feras Baig

Department of Civil and Environmental Engineering, Universiti Teknologi PETRONAS, Seri Iskandar 32610, Perak, Malaysia; firasbaig13@gmail.com

<sup>\*</sup> Correspondence: talhaansari510@gmail.com (M.T.Z.); raza.mustafa@utp.edu.my (M.R.U.M.)

**Abstract:** Natural landscapes have changed significantly through anthropogenic activities, particularly in areas that are severely impacted by climate change and population expansion, such as countries in Southeast Asia. It is essential for sustainable development, particularly efficient water management practices, to know about the impact of land use and land cover (LULC) changes. Geographic information systems (GIS) and remote sensing were used for monitoring land use changes, whereas artificial neural network cellular automata (ANN-CA) modeling using quantum geographic information systems (QGIS) was performed for prediction of LULC changes. This study investigated the changes in LULC in the Perak River basin for the years 2000, 2010, and 2020. The study also provides predictions of future changes for the years 2030, 2040, and 2050. Landsat satellite images were utilized to monitor the land use changes. For the classification of Landsat images, maximum-likelihood supervised classification was implemented. The broad classification defines four main classes in the study area, including (i) waterbodies, (ii) agricultural lands, (iii) barren and urban lands, and (iv) dense forests. The outcomes revealed a considerable reduction in dense forests from the year 2000 to 2020, whereas a substantial increase in barren lands (up to 547.39 km<sup>2</sup>) had occurred by the year 2020, while urban land use has seen a rapid rise. The kappa coefficient was used to assess the validity of classified images, with an overall kappa coefficient of 0.86, 0.88, and 0.91 for the years 2000, 2010, and 2020, respectively. In addition, ANN-CA simulation results predicted that barren and urban lands will expand in the future at the expense of other classes in the years 2030, 2040, and 2050. However, a considerable decrease will occur in the area of dense forests in the simulated years. The study successfully presents LULC changes and future predictions highlighting significant pattern of land use change in the Perak River basin. This information could be helpful for land use administration and future planning in the region.



**Citation:** Zeshan, M.T.; Mustafa, M.R.U.; Baig, M.F. Monitoring Land Use Changes and Their Future Prospects Using GIS and ANN-CA for Perak River Basin, Malaysia. *Water* **2021**, *13*, 2286. <https://doi.org/10.3390/w13162286>

Academic Editor: Achim A. Beylich

Received: 12 July 2021

Accepted: 12 August 2021

Published: 21 August 2021

**Keywords:** LULC; geographical information system; change detection; Perak River basin; cellular automata (CA) simulation; artificial neural network (ANN); future prediction; sustainable development

**Publisher's Note:** MDPI stays neutral with regard to jurisdictional claims in published maps and institutional affiliations.



**Copyright:** © 2021 by the authors. Licensee MDPI, Basel, Switzerland. This article is an open access article distributed under the terms and conditions of the Creative Commons Attribution (CC BY) license (<https://creativecommons.org/licenses/by/4.0/>).

## 1. Introduction

The process of determining changes in any process or object through analysis at different time periods is known as change detection [1]. Over time, humans have brought significant changes to the earth's surface to produce food through agricultural techniques. Nearly one-third of the surface of the earth is estimated to be agricultural, and over half of the earth's surface has been altered during the past few years [2]. This transition from naturally arising farming land to agricultural land is still underway [3]. These significant changes have drawn the attention of land use administrators and researchers to the influence of land use changes on hydrological processes [4]. Land use managers and decision makers can better understand the interactions between human and natural activities by examining the trends in change detection.

The assessment of LULC changes at various levels, such as global and regional, includes the evaluation of changes within river basins [5]. The tremendous growth in the

rate of population is the dominant factor at the global scale in the transition of land use, according to [6]. The drastic variations in land cover, especially in emerging countries, are mainly due to comprehensive urban development and the transformation of natural areas into industrial or agricultural lands [7]. The depletion of natural land, thick forests, and watersheds puts considerable pressure on the hydrological regimes and mechanisms of river basins [8]. It is important to provide multi-temporal sets of data for the evaluation of changes in the spatial characteristics of land [9]. The use of multi-temporal datasets makes it simple to explain the major LULC changes along with their pattern [10]. The advancement of computer technologies and the introduction of Landsat satellites have made it simpler to trace the changes and advancements that have occurred over the last several decades. Remote sensing technology linked with a GIS has been usefully implemented in the identification of multiple environmental characteristics, i.e., vegetation covering, urban sprawls, transition in forests, and particularly variations in LULC changes for certain time periods [11]. It has been observed that remote sensing and GIS techniques offer more accurate and cost-efficient data evaluation in comparison to other traditional approaches and surveys [7]. Remote sensing is defined as observing spatial variations in different objects without physical interaction with them. To classify the various characteristics of the earth, remote sensing uses space-borne satellites. Because of their frequent monitoring of the earth's features, they have the ability to assist in tracking changes on the land surface [12]. The information gained on temporal and spatial levels allows scientists and researchers to recognize the large-scale changes in pattern of land and permits regional policymakers and authorities to make future decisions. The application of remote sensing in natural disaster management has been reported in many studies. It had been used for monitoring floods in India [13]. Geomorphic factors were examined for the establishment of a decision support system by [14] in order to avoid the occurrence of landslides using remote sensing. Furthermore, it has proved useful in identifying changes in agricultural patterns, land cover changes, and urban sprawls [15]. GIS are regarded as essential for identifying the changes in remotely sensed images [16]. It offers the ability to integrate data from multiple resources for the identification of change. The combined effect of the hydrological maps, soil and topographic maps, and classified images obtained through GIS may provide helpful information in extracting land use for a given area. In addition, it may show the tendencies of land use changes because of its ability to develop the model by using provided statistics and datasets. Moreover, GIS and remotely sensed images are widely utilized to recognize LULC changes [17–19]. For tracking land cover changes, the combined use of GIS and remote sensing has been demonstrated to be a reliable and profitable technique [20–23]. The efficacy of space-borne imaging in mapping LULC changes has been demonstrated in many studies [24,25]. Several Landsat images of various time spans (1972–2008) have been used by [26] to investigate the land use and land cover changes in Egypt. In order to examine LULC changes in Rwanda, [27] used Landsat images from various years (1987–2016). The recent study by [28] analyzed LULC changes in Kenya by using GIS and remote sensing techniques. Similarly, numerous studies have been reported to observe LULC changes in different catchments in Malaysia [29–31].

For the forecasting and simulation of LULC changes, a wide range of models have been developed so far [32–34]. For land use modeling, statistical-based methods and machine learning methods have also been used for decades [35,36]. These methods statistically describe the relationships between variables [33]. Markov chain analysis (MCA) or Markov models [37], cellular automata (CA) [38], cellular automata–Markov models (CA–Markov) [39], artificial neural networks (ANNs), binary logistic regression, and fractal models [40,41] are among the most common models used for simulation and prediction of LULC changes [42]. For LULC simulation, CA constitute an appropriate and commonly used model [32]. However, it appears from the literature that so far, no study has been conducted for prediction of LULC changes in the Perak River basin. The combination of ANN-CA for prediction of LULC changes has also not been utilized for this region. Performing such a study is imperative, and its outcomes could be helpful for regional

policymakers and authorities in making decisions for future monitoring and planning. Therefore, in this study, ANN-CA simulation was used to forecast the land cover change scenarios for the Perak River basin until the year 2050.

The Perak River basin is an important asset to the people in the region and the primary source of raw water in the region. Hence, the sustainability of the environment in and around the Perak River basin is important, as urbanization is one of the possible challenges to the sustainable growth of the region. Therefore, the aim of this study was to examine the LULC changes in the Perak River basin of Malaysia from the years 2000, 2010, and 2020 with the specific objectives to measure the extent and causative factors of land use in the Perak River basin over the given time span. ANN-CA simulation was employed to determine the future aspects of LULC changes in the Perak River basin for the years 2030, 2040, and 2050.

## 2. Materials and Methods

### 2.1. Study Area

Perak is situated in the western part of peninsular Malaysia, bordered to the north side by Kedah and the south coast of Thailand, to the northwest by Palau Penang, to the east by Kelantan and Pahang, and to the south by Selangor, and occupies an area of 21,035 km<sup>2</sup>. It ranges geographically from 3°30' N to 6°0' N longitude and 100°0' E to 102°0' E latitude, as shown in Figure 1 [31]. The shapefile of the study area was obtained from a website providing data-interpolating variational analysis (DIVA-GIS) (Retrieved on 27 February 2021, <https://gadm.org/maps/MYS.html>) from which study area map was clipped. The second-largest river basin in peninsular Malaysia is the Perak River basin. It occupies about 70% of the state of Perak and has a river basin area of approximately 14,908 km<sup>2</sup>. Its reservoirs occur between the Perak–Kelantan–Thailand mountainous areas, bordering the Belum forest in the north of the region. Sg. Pelus, Sg. Kinta, Sg. Batang Padang, and Sg. Bidor are the main tributaries in the surrounding area. River system communities inhabited along the main river include Lenggong, Kuala Kangsar, Gerik, and Parrit. The range of temperature in the Perak River basin is from 22 °C to 35 °C, with sunny days and cold nights all around the year. The rate of humidity varies from 80 to 82% annually, which is relatively high. The mean annual precipitation is recorded to be 3200 mm.

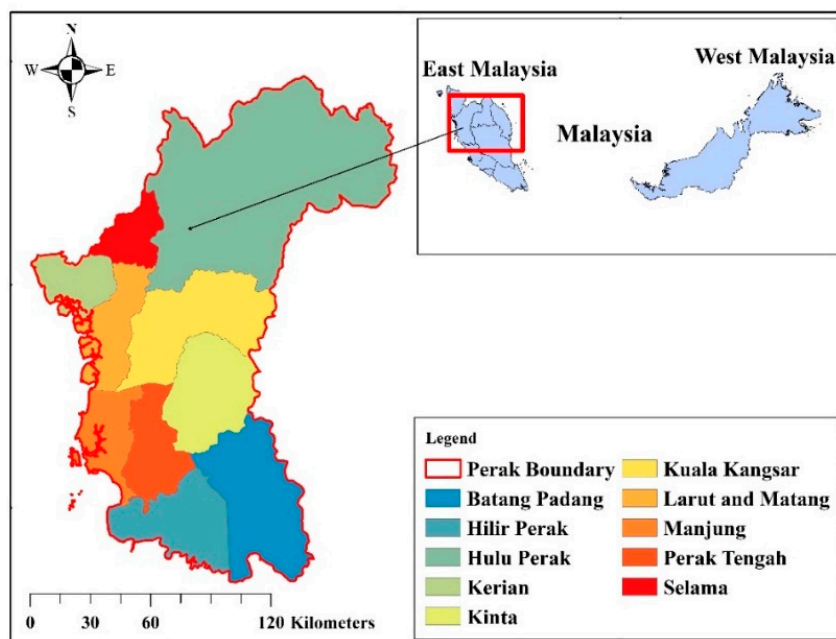


Figure 1. Description of the study area.

The United States Geological Survey (USGS) earth explorer website was used for acquiring the digital elevation model (DEM) from which the elevation data of this study area were extracted, as shown in Figure 2. The radar system collects information that results in the most precise and detailed topographical map of the surface of Earth ever produced. The Perak River basin area consists primarily of gentle, elongated highlands with mild to steep slopes. The study area has a range of elevation between 27 m and 2168 m above mean sea level (MSL). From Figure 2, it can be observed that areas towards the north side such as Hulu Perak, Kuala Kangsar, Kinta and Batang Padang have the highest elevation rates above mean sea level. Regulations for planning and development in hilly and highlands regions have been established by the government of Malaysia. The regulations were categorized into various elevation ranges: lowlands (less than 150 m), hilly lands (150–300 m), highlands (300–1000 m), and mountainous lands (more than 1000 m). The elevation of the study area is directly proportional to the steepness of slopes, which has a direct connection with soil erosion rate [43].

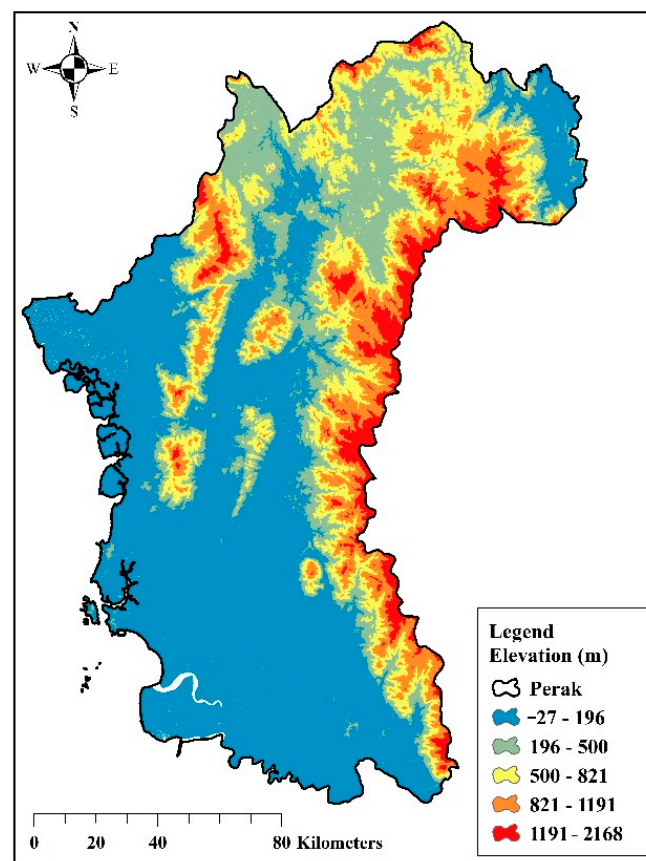
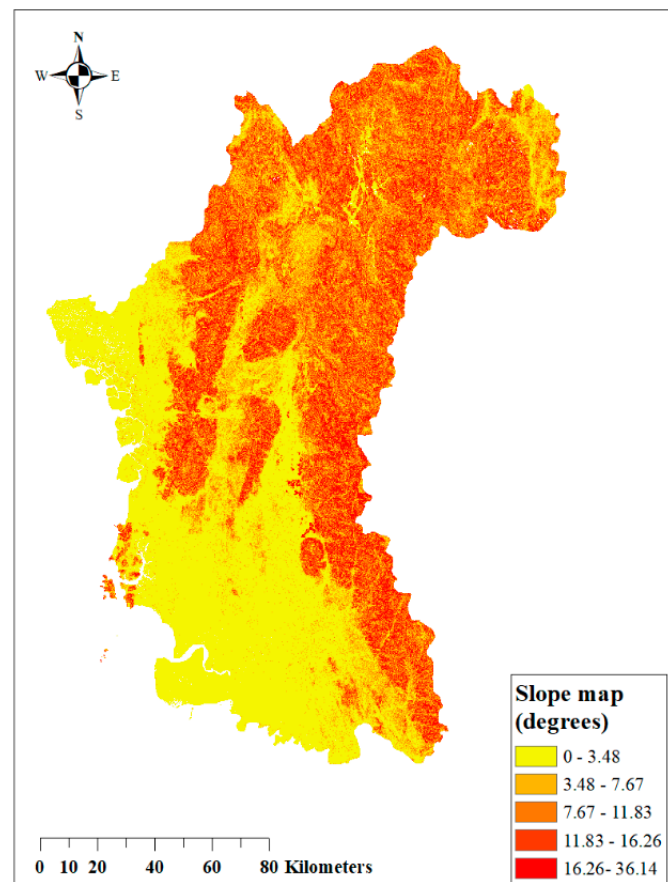


Figure 2. The elevation map of the study area.

A slope map of the study area was made in order to estimate the steepness of the region. From the slope map, five classes of distinct steepness were generated. The variation in steepness was based on the topographical features of the study area. The main ranges of steepness in the five classes of the study area were from  $0\text{--}3.48^\circ$ ,  $3.48\text{--}7.67^\circ$ ,  $7.67\text{--}11.83^\circ$ ,  $11.83\text{--}16.26^\circ$ , and  $16.26\text{--}36.14^\circ$ , as shown in Figure 3. The factor of slope steepness has a significant effect on the rate of soil erosion, soil stability, and sedimentation. The amount of soil erosion increases with the increase in slope gradient due to a rise in the velocity of surface runoff [44].



**Figure 3.** Slope map of the study area.

## 2.2. Data Acquisitions and Preparation

Landsat images acquired from Landsat 5 and Landsat 8 satellites were utilized to analyze the LULC changes, whereas dates were chosen focusing on the quality and accessibility of Landsat data and weather conditions, as shown in Table 1. The data for Landsat 5 and Landsat 8 showed a minimal consistency issue from the perspective of spatial composition. These issues were rectified during pre-classification phase of the analysis and have been successfully addressed by some previous studies [4–6] as well. The visible bands (red, green, and blue) were selected for land use classification. The bands selected for Landsat 5 classification were 2, 3, and 4, whereas 4, 5, and 6 bands were selected for Landsat 8 image classification [45]. Four Landsat images were obtained for the years 2000, 2010, and 2020 from the USGS earth explorer website (Retrieved on 27 February 2021, <https://glovis.usgs.gov>) using Path/Row 127/56, 127/57, 128/56, and 127/57 for the Perak River basin (Table 1). The datasets were added to ArcGIS to generate LULC maps. The ArcGIS 10.8 software package was used at the different stages of the analysis. The images obtained from the satellite were sensed at various times of the year and all had the same spatial resolution (30 m). The resulting four images were clipped to extract the study area, after checking the Landsat scene by date.

**Table 1.** Detailed data for the Landsat images used for the study area.

Year	Landsat Scene ID	Path	Date Acquired	Resolution (m)	Row	Earth-Sun Distance
2000	LT51270562000237BKT00	127	24 August 2000	30	56	1.0109543
	LT51270572000237BKT00	127	24 August 2000	30	57	1.0109543
	LT51280562000020DKI00	128	20 January 2000	30	56	0.9839503
	LT51280572000148BKT01	128	27 May 2000	30	57	1.0132773
2010	LT51270562010056BKT00	127	25 February 2010	30	56	0.9898357
	LT51270572010360BKT00	127	26 December 2010	30	57	0.9834906
	LT51280562010047BKT00	128	16 February 2010	30	56	0.9878930
	LT51280572010047BKT00	128	16 February 2010	30	57	0.9878930
2020	LC81270562020228LGN00	127	15 August 2020	30	56	1.0128081
	LC81270572020228LGN00	127	15 August 2020	30	57	1.0128080
	LC81280562020315LGN00	128	10 November 2020	30	56	0.9902608
	LC81280572020267LGN00	128	23 September 2020	30	57	1.0034227

### 2.3. Classification

In order to achieve high precision of classification, false color composites and indexes of water and vegetation were produced with normalized differences. For improved visualization, the mixture of green, near-infrared (NIR), and red bands (R) was the false color composite that was utilized. Moreover, *NDVI*, i.e., normalized difference vegetation index, and *NDWI*, i.e., normalized difference water index, were created for all images. The usage of *NDVI* in estimation of vegetation covering has been effectively in past years for different purposes [46]. It can be described by Equation (1):

$$NDVI = \frac{NIR - R}{NIR + R} \quad (1)$$

where *NIR* and *R* indicate the reflectance of the surface over nearly 0.8  $\mu\text{m}$  and visible band (0.6  $\mu\text{m}$ ) in the spectrum of light, respectively. Normalized difference water index (*NDWI*) as shown in Equation (2), on the other hand, demonstrates the maximum water reflectance around an area by using the visible green band (*G*) (0.5  $\mu\text{m}$ ) and the near-infrared band (*NIR*) (0.8  $\mu\text{m}$ ) [47–49].

$$NDWI = \frac{G - NIR}{G + NIR} \quad (2)$$

False color images helped in detection and visualization of different land characteristics, while *NDVI* and *NDWI* were used to distinguish the vegetative and water surfaces, respectively, in the study area. The supervised classification technique has been used effectively in the case of spectral variability in individual types of cover, and hence it was applied for the digital classification of Landsat images [50]. Supervised classification yields superior results in comparison to unsupervised classification, as shown by many recent studies [51,52]. All the satellite images were analyzed by applying per-pixel signature to the same digital number (DN) of various landscape features and used to distinguished the study area into four classes. The defined classes were dense forests, barren and urban lands, waterbodies, and agricultural lands, as shown in Table 2. Training samples were selected by defining polygons around the representative locations for each of the predetermined LULC types. An appropriate spectral signature is one that helps to ensure that there is negligible confusion between land covers that are to be mapped [53]. A total of 120 spectral signatures for each class were captured; therefore, an accumulated 480 training points from all four classes were selected. Then, the signature files were created, which are representative of a class or a cluster. After the creation of signature files, they were added with the base map, which provides the background of the geographical context of the study area.

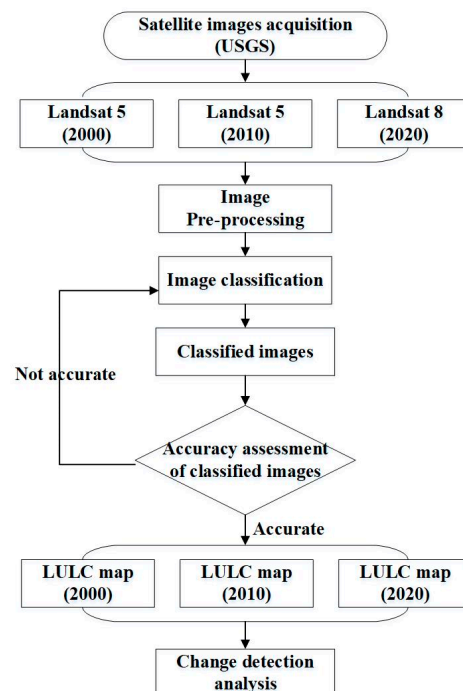
**Table 2.** The classification scheme for land use and land cover (LULC).

Class	Description
Waterbodies	Rivers, open water, lakes, ponds, and reservoirs.
Barren and urban lands	Land areas of exposed soil and barren areas influenced by humans.
Dense forests	Continuous stands of trees, many of which may attain a height of 50 m, including natural forest, mangrove, and plantation forest.
Agricultural lands	Mainly composed of grass, vegetation, crop plants, cultivated lands, and shrub lands.

Later, for the supervised classification of the Landsat images, the maximum-likelihood classification technique was applied. With this classification method, selection of pixel values related to different classes can be controlled by the user [54]. The outcomes obtained from the supervised classification and images of higher resolution show the classification of the study area. Then, kappa coefficient was calculated for the accuracy assessment of classified maps. The kappa coefficient is an accuracy indicator for measuring the overall coherence between the classified images and reference data. Multi-separate variables technique was used to calculate kappa coefficient, which was used to measure the accuracy of classified maps. It was derived from the confusion matrix that relates the classification map and referenced data [55]. The kappa coefficient was calculated by using Equation (3) [56]:

$$K = \frac{N \sum_{i=1}^m CM_{ii} - \sum_{i=1}^m Ci_{corr}Ci_{pred}}{N^2 - \sum_{i=1}^m Ci_{corr}Ci_{pred}} \quad (3)$$

where  $K$  represents Cohen's kappa coefficient,  $Ci_{corr}$  represents the corrected random samples in rows of confusion matrix,  $Ci_{pred}$  represents the predicted random samples in columns of confusion matrix of each class,  $CM_{ii}$  represents the diagonal elements of the confusion matrix, and  $n$  represents the total number of random samples. The flow chart of all the processes involved in the methodology is shown in Figure 4.

**Figure 4.** Detailed flow chart of methodology.

#### 2.4. Change Detection

Change detection is considered as a primary method for identifying the variations in land use pattern of different classes (i.e., waterbodies, barren and urban lands, agricultural lands, and dense forests) in distinct periods of time. The essential characteristic of this method is the capacity to identify the changes in data from various sources and time spans [57]. Change detection was calculated by finding the difference in the area covered by different land use classes between the two periods of 2000 to 2010 and 2010 to 2020. For the calculation of area covered by different land use classes, the “attribute table” was obtained after the land use classification was analyzed. The pixels covered by each class were divided by the total pixels of the study area to obtain percentage change in cover for each class, as shown in Equation (4) [58].

$$\text{Percentage cover (\%)} = \frac{\text{pixels covered by land use class}}{\text{total pixel of the study area}} \times 100 \quad (4)$$

#### 2.5. Artificial Neural Network–Cellular Automata Modeling

During the last two decades, several models based on simulations have been developed that are used for the modeling of land cover changes around the globe [59]. In this study, a combination of ANN and CA was used to simulate and evaluate the LULC trends of the Perak River basin up to the year 2050 using open source QGIS software version 2.18.25 [60]. The CA feature in QGIS is based on the Markov chain algorithm; i.e., it relies on the present state of land use rather than the previous state [15]. This model generates the output data in the form of tables and maps by combining previous and current land use maps with spatial input parameters [61]. Based on that data, MOLUSCE uses algorithms to train the model. Since ANN algorithms are more accurate than other algorithms, it was used to train the transition potential model of LULC [60]. In recent decades, ANNs have become most common in remote sensing for proper LULC modeling and classification [62]. An ANN is composed of neurons, which are the same as those found in the brains of humans, and it uses them to recognize the trends in data [63]. The most popular form of ANN is the multilayer perceptron (MLP) [64]. The MLP-ANN preprocesses the provided data from land use groups such as barren and urban lands, water bodies, and agricultural lands by using dummy coding of different groupings into a collection of independent variables such as 0 and 1.

The transition potential model used in this study was trained with a momentum of 0.050 and a learning rate of 0.100 for the stabilization of learning graph. Furthermore, the number of iterations was set to 100 to prevent the issue of overfitting in the model. ANN-CA simulation was utilized to simulate the land use changes. The state of the new cell was determined by the existing state of a current cell and changes in the neighborhood cells in CA [65,66]. The ANN-CA simulation selects raster data, such as classes of LULC, raster of spatial parameters, and transition potential model, based on ANN algorithm [67]. Potential changes are determined for each class, and the simulation creates a raster of the most likely transitions. The simulation examines a fixed number of pixels, with the greatest certainty for each transition corresponding to the most likely transitions, and then adjusts the class of the pixel [68]. Multiple iterations of the simulation were performed to achieve subsequent prediction maps of 2030, 2040, and 2050.

Validation was conducted after the ANN-CA simulation, which allows for verifying, comparing, and validating the outcomes achieved. The method of validation was carried out by comparing simulated outcomes to the reference data [68]. Calibration and validation processes are critical factors in validating a simulation model, and [69] stated that there is a clear distinction between these two terms. The predicted map of 2020 was obtained by inserting classified maps of 2000 and 2010 as input data. The predicted map of 2020 was compared with the observed classified map of 2020 to assess the degree of agreement between the pixels of the two maps. The overall kappa coefficient was calculated, the value of which ranges from 0 to 1 [15]. The high degree of agreement and satisfactory



value of kappa coefficient indicated the validation of the simulation model. This validated simulation model formed the basis for future predicted maps of 2030, 2040, and 2050. The detailed methodology flow chart of prediction maps is shown in Figure 5.

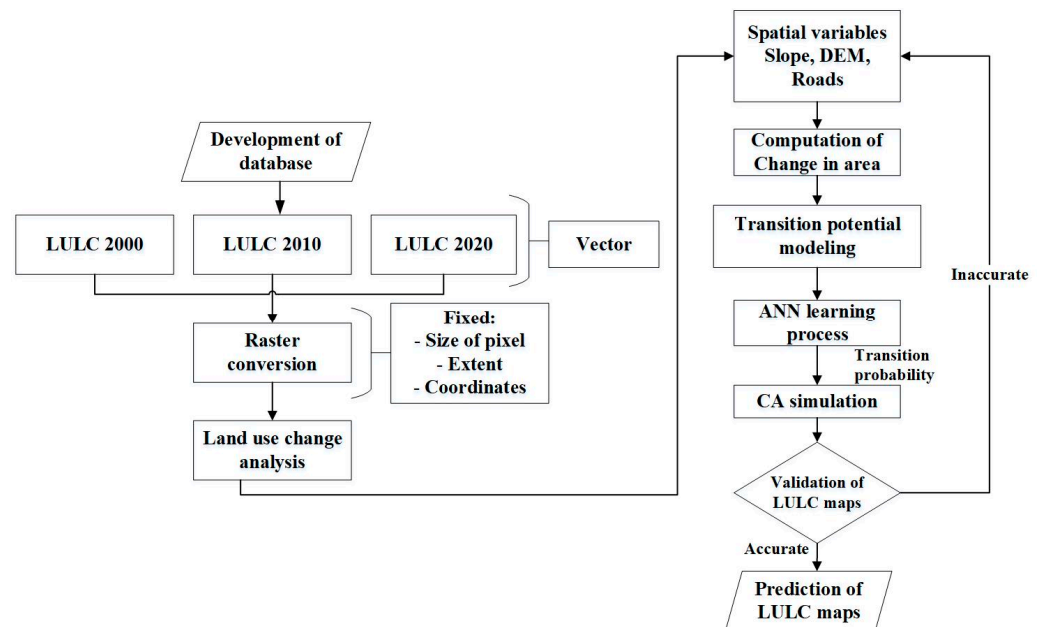


Figure 5. Flow chart of future LULC prediction mapping.

### 3. Results and Discussions

#### 3.1. Land Use Change and Accuracy Assessment

The spatial representation of LULC types of four major classes of land cover, namely (i) waterbodies, (ii) agricultural lands, (iii) barren and urban lands, and (iv) dense forests, from the year 2000 to 2020 is shown in Figure 6a–c. These figures illustrate the land use condition in the Perak River basin. Firstly, for the composition of the band, Landsat images were inputted into an image analysis tool. Then, by using Landsat images, the signatures of all the spectral classes were identified. For the purpose of supervised classification, the classes with the same spectral signatures were merged. This allows all the pixels that are included in an image to be automatically assigned to the land cover classes [70]. The maximum-likelihood classifier was employed by applying training sets developed from Landsat images.

The accuracy assessment of the classified images was the next stage after classification. The stratified samplings were generated by using Google Earth images, and then accuracy assessment of LULC maps was performed. Confusion matrix was created between testing samples and classified images for the measurement of accuracy. It is a simple way to evaluate how frequently a pixel misidentifies class [15]. For the formation of confusion matrix table, 189, 202, and 177 random points were selected on the classified maps for years 2000, 2010, and 2020 respectively (Table 3). These random points represented different land use classes that were compared with Google Earth images. These random points represented the producer's values and user's corrected values. The dataset table was transformed into a confusion matrix by comparing the total producer's values and the user's corrected values in the respective classes. According to Anderson's classification scheme, the kappa values of classified images are considered satisfactory if they reach the minimum accuracy of 0.85 [45]. Several attempts were made by increasing training sample size to enhance accuracy until reaching kappa coefficient of more than 0.85 as the desired accuracy. The overall accuracies of classified images for the years 2000, 2010, and 2020 were 0.86, 0.88, and 0.91 respectively, as shown in Table 3. Additionally, the table also describes the accuracy of each class for all the images. Based on the outcomes shown in

the table, it is apparent that the accuracy of classification of waterbodies (96%) is relatively higher as compared to agricultural and barren land in the year 2000. This is because the forests and waterbodies represent clear pixels and make the process of classification simple [71]. In comparison to this, the accuracy of the barren and agricultural classes was comparatively poor due to the mixed environmental characteristics. The accuracy assessment for all images indicates that it is difficult to determine agricultural lands and areas with fewer forests with high precision due to the spatial resolution restrictions of the Landsat images. The existence of waterbodies and farmlands in barren areas contributes to a rise in the amount of mixed pixels. For appropriate mapping of agricultural and barren lands, ancillary data and visual representation of images was used. For the classified images of the years 2010 and 2020, the confusion matrix in Table 3 demonstrates the increase in accuracy of classifications. The accessibility of ancillary data for the classification was the reason for the enhancement of accuracy. The accuracy for agricultural and barren land classification also improved due to the interconnection of various data sources, i.e., the data from Google Earth and Landsat images data. These findings offer a significant foundation for the future study of LULC changes.

**Table 3.** Accuracy assessment of the LULC classifications in the Perak River basin.

2000	AL	W	BL	DF	Total	UA (%)
AL	36	0	1	3	40	90
W	0	47	1	1	49	96
BL	1	2	49	4	56	87
DF	3	0	2	39	44	89
Total	40	49	54	47	189	
PA (%)	90	95	91	83		
OA (%)	90					
K	0.86					
2010	AL	W	BL	DF	Total	UA (%)
AL	55	0	1	3	59	93
W	0	42	1	1	44	95
BL	4	2	57	1	64	89
DF	3	0	0	32	35	91
Total	62	44	59	37	202	
PA (%)	89	94	97	86		
OA (%)	92					
K	0.88					
2020	AL	W	BL	DF	Total	UA (%)
AL	61	0	0	2	63	97
W	0	45	0	0	45	100
BL	3	0	27	0	30	90
DF	2	0	1	36	39	92
Total	66	45	28	38	177	
PA (%)	92	100	96	95		
OA (%)	95					
K	0.91					

Note: AL = Agricultural lands; W = Waterbodies; BL = Barren and urban lands; DF = Dense forests; UA = User's accuracy; PA = Producer's accuracy; OA = Overall accuracy; K = Kappa coefficient.

### 3.2. Land Use Changes in Perak River Basin

The details of land use changes in the Perak River basin for the years 2000, 2010, and 2020 are given in Tables 4 and 5, as well as Figure 7. In the year 2000, the major land cover in the study area was occupied by dense forests comprising 56% of the total area, followed by agricultural lands (27.73%), barren and urban lands (14.63%), and waterbodies (1.62%). Compared to the year 2000, in 2010, the land cover experienced a tremendous decrease in dense forests (43.69%), followed by a considerable increase in barren and urban lands (15.71%) as well as a slight increase in the area of waterbodies (1.68%) and

agricultural lands (39.05%). However, for the year 2020, the observed LULC changes were dominated by a sizeable increase in the area of barren and urban lands (20.39%), followed by a dramatic decrease in dense forests (35.47%) and a slight increase in waterbodies (1.75%) and agricultural lands (42.46%), as shown in Table 4.

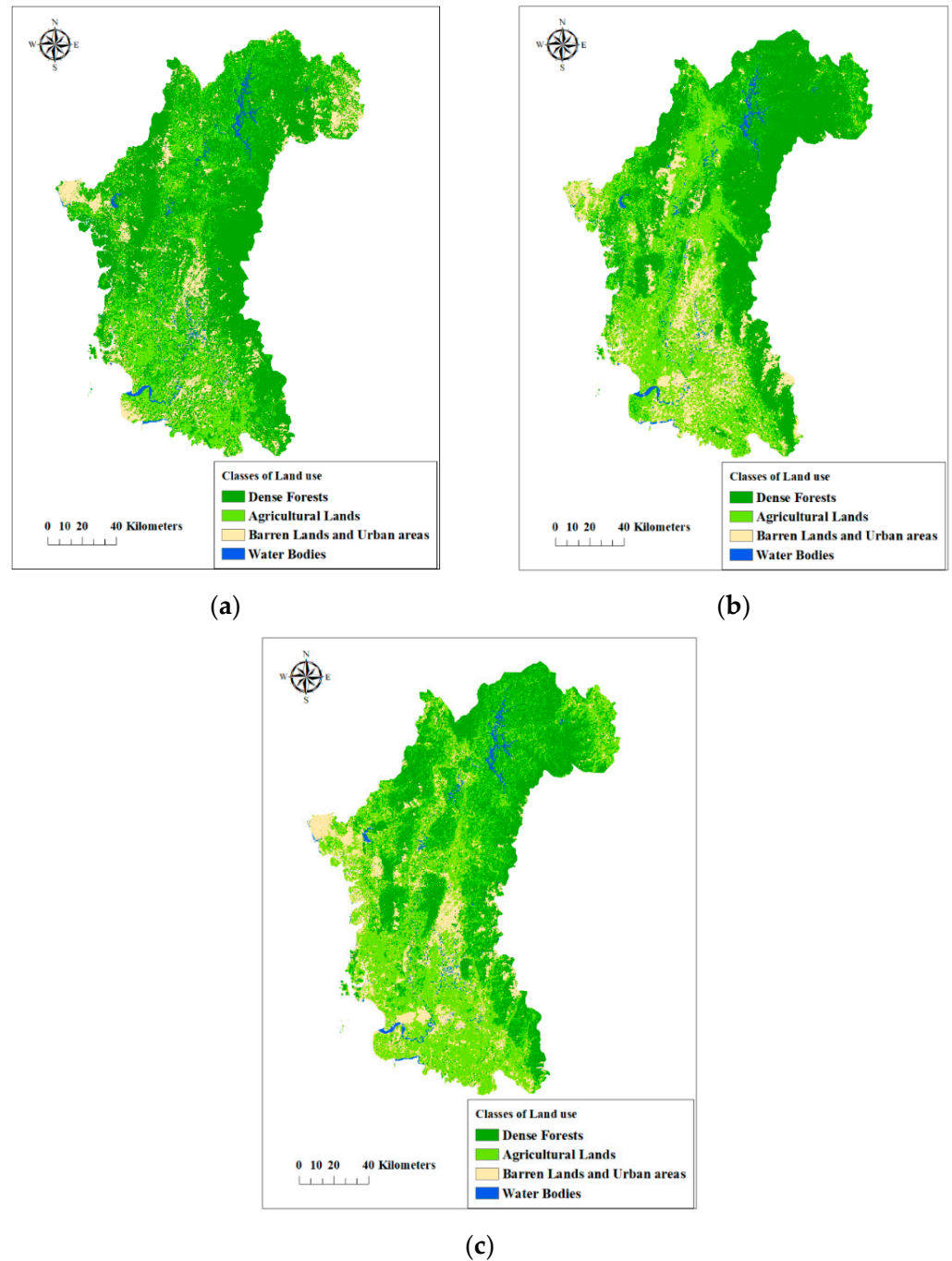


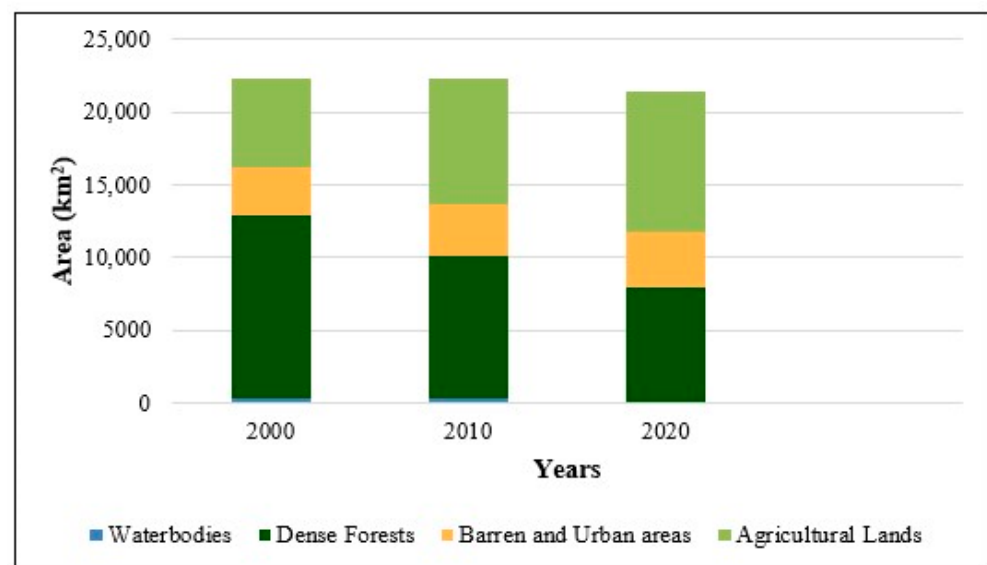
**Figure 6.** Land use and land cover classifications of Perak River basin for: (a) year 2000; (b) year 2010; and (c) year 2020.

**Table 4.** Outcomes of the classification of LULC for images from the years 2000, 2010, and 2020, demonstrating the area of each class and its percentage of the Perak River basin.

Years	2000		2010		2020	
LULC (Area)	Area (km <sup>2</sup> )	%	Area (km <sup>2</sup> )	%	Area (km <sup>2</sup> )	%
Dense Forests	12,512.30	56.02	9739.54	43.59	7925.04	35.47
Agricultural Lands	6195.98	27.73	8714.08	39.04	9603.39	42.46
Barren and Urban Lands	3270.01	14.63	3510.39	15.71	3817.07	20.29
Waterbodies	363.18	1.62	377.47	1.68	391.79	1.75

**Table 5.** Changes in area and percentage cover of LULC classes between the years 2000–2010, and 2010–2020 of the Perak River basin.

Years	2000–2010		2010–2020	
LULC (Area)	Area (km <sup>2</sup> )	%	Area (km <sup>2</sup> )	%
Dense Forests	−2772.77	−12.4108	−1812.85	−8.11
Agricultural Lands	2518.09	11.27	889.90	3.46
Barren and Urban Lands	240.38	1.07	307.36	4.59
Waterbodies	14.29	0.06	15.31	0.068

**Figure 7.** LULC change graph for 2000, 2010, and 2020 for Perak River basin.

The main factors contributing to the increase in barren and urban lands in the Perak River basin were rapid expansion of urban development, the increase in the growth of agricultural cultivation that eventually contributed to the degradation of forest, and the variation in the amount of annual rainfall [72–74]. Such LULC change analysis is important for a deeper understanding of how these developments were changing the hydrological process of the Perak River basin. Remotely sensed image integration with GIS has the ability to provide a good basis for comparing the influencing factors to the dynamics of the river basin. The outcomes obtained from the analysis have shown that in the last two decades, the land use in Perak, Malaysia has been changed. The main components of

the river basin have been decreased dramatically, such as dense forests. Barren land, by comparison, has seen more changes and increased more considerably than any other class of land use. Due to the increase in barren and urban land, the huge number of light forests have been converted into development zones, and thus the area of impermeable surfaces has been enhanced [75]. The rapid urbanization was mainly due to industrial development and growth in the rate of population. A slight positive increase was detected in the class of waterbodies in the year 2010, which can be attributed to the rise in water bodies, such as reservoirs that perform the function of retention ponds in the season of floods. Increases in barren lands and rainfall played significant roles in changing the hydrological system of the river basin [76–78]. Precipitation over recently built areas results in increased rates of runoff, which creates the issue of floods in the low-lying region, according to various studies [79]. Additionally, in urban areas where the capacity for flood retention and drainage is not adequate, heavy rainfall may also lead to an increase in stagnant water. Factors influencing the river basin, i.e., change in climate, land use, and changes in soil infiltration rate, may also result in significant deterioration of the river basin hydrological process [80]. Therefore, the analysis of land use changes can also provide key details on potential improvements to the hydrology of the river basins.

### 3.3. Prediction of Land Use Changes Using ANN-CA

#### 3.3.1. Transition Potential Modeling Using ANN

The transition potential model was trained using an ANN for identifying LULC changes between the years 2000 and 2010. The changes in the area of different classes were used to create the LULC transition matrix, which is an input for the ANN to obtain the transition probability. The ANN was run with the learning rate of 0.09 and a maximum iteration of 100, and momentum was set to 0.050. These inputs were found to be optimal to train the ANN. ANN-CA simulated the prediction map of 2020 based on the transition potential model and spatial parameters.

#### 3.3.2. Validation of ANN-CA Simulation

The simulation results were statistically validated by kappa coefficient and percentage of correctness. The kappa coefficient was calculated using the guidelines in QGIS [60]. The same method of validation has been successfully used in the previous studies concerning land use prediction using ANN-CA simulation [15,81]. The parameters used for validation were obtained from the simulated and classified reference maps of 2020. The comparison of these maps produced the kappa coefficient and percentage of correctness. The value obtained for the kappa coefficient was 0.83. The graph shown in Figure 8 represents the comparison and correlation between the predicted and reference maps of 2020. The validation graph tracks the agreement between data points of the two maps, which suggests an accurate prediction has been conducted, whereas a divergence from the reference line signifies the inaccurately simulated land cover. The minimal errors related to the simulation can be attributed to the inaccurate identification of land use patterns and misinterpretation of spatial parameters (i.e., network of roads, elevation, and slope maps). Similar trends have been reported during the validation of simulated maps in previous studies [61,81,82].

The predicted maps of 2030, 2040, and 2050 were obtained by implementing multiple iterations of the validated simulation results of 2020. The percentage correctness of the simulation was 73.41%. The percentage of correctness suggests that there would be a 73.41% chance of correctness in predicted outcomes of 2030, 2040, and 2050 simulations when compared with the actual LULC maps of 2030, 2040, and 2050. It also indicates that if the current LULC changes would proceed in the same trend, then the future land use pattern for the Perak River basin would be comparable to the maps shown in Figure 9.

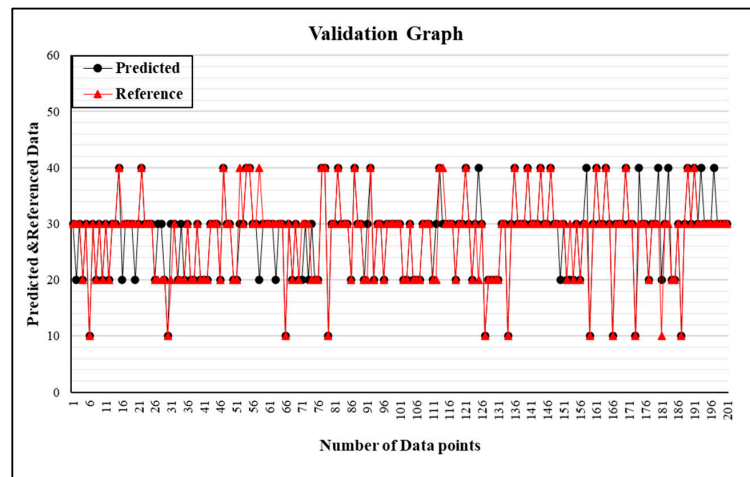


Figure 8. Validation graph of predicted and referenced data points.

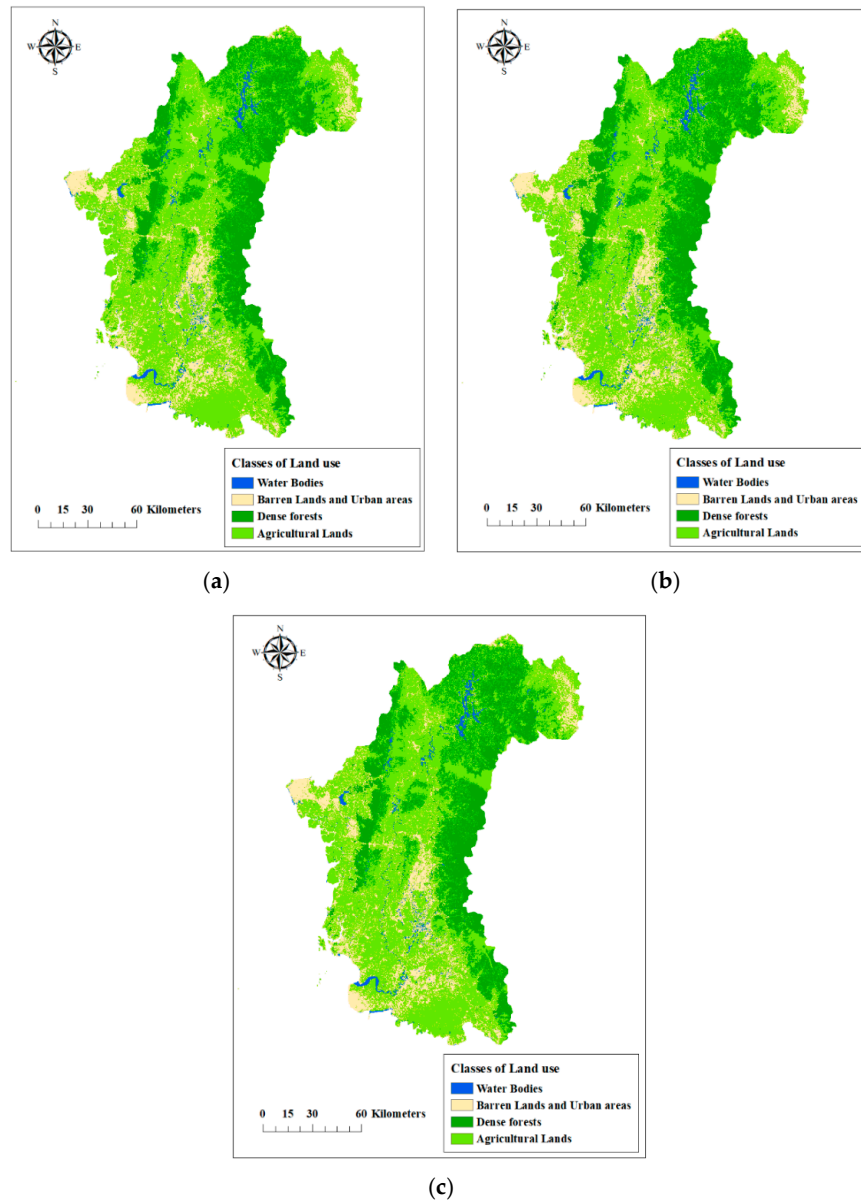


Figure 9. Predicted LULC of Perak River basin for: (a) year 2030; (b) year 2040; and (c) year 2050.

### 3.3.3. Prediction Maps of Year 2030, 2040, and 2050

The outcomes of ANN-CA simulation as shown in Figure 9 illustrate that the Perak River basin will see a slight increase in areas of barren lands and agricultural lands in the years leading to 2030, 2040, and 2050. Based on the simulation results, there will be a minor decrease in the area of waterbodies of ( $-1.56 \text{ km}^2$ ) between the years 2030 to 2040 and ( $-2.53 \text{ km}^2$ ) from the year 2040 to 2050 due to the expected increases in bedload and sedimentation in the flood retention ponds and rainfed catchments, as shown in Table 6. Similarly, an increase in the area of agricultural lands of ( $60.6 \text{ km}^2$ ) was predicted from the year 2030 to 2040 and ( $46.9 \text{ km}^2$ ) from the year 2040 to 2050. However, dense forests will decrease ( $-335.91 \text{ km}^2$ ) from the year 2030 to 2040 and ( $-94.77 \text{ km}^2$ ) from the year 2040 to 2050 due to the expected increase in rates of deforestation and conversion of forests into developed areas. Similarly, there will be an increase in the area of barren and urban lands ( $65.95 \text{ km}^2$ ) from the year 2030 to 2040 and ( $51.24 \text{ km}^2$ ) from the year 2040 to 2050 due to an expected increase in commercial, residential, and industrial areas.

**Table 6.** Projected land use and land cover changes for the years 2030, 2040, 2050.

Class Name	Area ( $\text{km}^2$ ) 2030	Area ( $\text{km}^2$ ) 2040	Area ( $\text{km}^2$ ) 2050	Change from 2030 to 2040 ( $\text{km}^2$ )	Change from 2040 to 2050 ( $\text{km}^2$ )
Waterbodies	388.72	387.16	384.633	-1.56	-2.53
Barren and urban lands	3830.35	3896.3	3948.24	65.95	51.24
Dense forests	7461.2	7125.39	7030.62	-335.91	-94.77
Agricultural lands	9788.3	9847.8	9894.7	60.6	46.9

### 3.3.4. Land Use Transition Matrix of Simulated Outcomes

A transition matrix table illustrates how future land use classes may change during the periods of 2020–2030, 2030–2040, and 2040–2050. The transition matrix table was formed by comparing the observed classified map of 2020 with the simulated map of 2030, and similarly comparing the simulated map of 2030 with 2040 and 2040 with 2050. The transition matrix indicates the changes in land use patterns in the simulated years. The observed changes in land use classes are shown in Table 7. From the table, it is evident that from 2020–2030, the major transition occurs in dense forest to agricultural lands. Similarly, there is a shift of agricultural lands to barren and urban lands. However, minor transformations occur in the classes of waterbodies, barren and urban lands. This trend of changes in the land use patterns remains constant in the years leading up to 2040 and 2050.

**Table 7.** Land use transition matrix of the year 2030, 2040, and 2050.

	2020–2030			
	Waterbodies	Barren and Urban Lands	Dense Forests	Agricultural Lands
Waterbodies	0.90	0.06	0.03	0.01
Barren and urban lands	0.00	0.94	0.01	0.05
Dense forests	0.00	0.06	0.75	0.19
Agricultural lands	0.00	0.12	0.05	0.83

Table 7. Cont.

2030–2040				
	Waterbodies	Barren and Urban Lands	Dense Forests	Agricultural Lands
Waterbodies	0.96	0.00	0.00	0.04
Barren and urban lands	0.00	0.98	0.01	0.01
Dense forests	0.00	0.02	0.87	0.11
Agricultural lands	0.00	0.03	0.06	0.91
2040–2050				
	Waterbodies	Barren and Urban Lands	Dense Forests	Agricultural Lands
Waterbodies	0.97	0.00	0.01	0.02
Barren and urban lands	0.00	0.95	0.01	0.04
Dense forests	0.00	0.02	0.85	0.13
Agricultural lands	0.00	0.07	0.05	0.88

#### 4. Conclusions

The present study has successfully provided an application of ANN-CA for the monitoring and prediction of LULC changes and spatial distribution patterns. The growth in LULC changes and future prediction of the Perak River basin were analyzed by using multi-temporal data from the year 2000 to 2020. The LULC changes maps classified for the years 2000, 2010, and 2020 demonstrated the major changes in the study area. Furthermore, areas of various LULC classes were calculated to monitor decadal changes in each class. According to the findings, barren and urban lands in the Perak River basin grew rapidly between 2000 and 2020. In 2000, the total area of barren and urban lands in the region was 3270.01 km<sup>2</sup>, which had increased up to 3817.07 km<sup>2</sup> by the year 2020, leading to extreme soil erosion risk in the catchment. This shows that there was an approximately five-fold increase in barren and urban lands during this period of time. The decadal change in LULC mapping of the Perak River basin indicated that the dense forests significantly decreased from 12,512.30 km<sup>2</sup> in the year 2000 to only 7925.04 km<sup>2</sup> in 2020. However, a slight increases were observed in the areas of waterbodies, from 363.18 km<sup>2</sup> in 2000 to 391.89 km<sup>2</sup> in 2020, and agricultural lands, from 6195.98 km<sup>2</sup> in 2000 to 9603.39 km<sup>2</sup> in 2020. Dense forests near the Perak River basin were transformed into non-agricultural lands initially and later converted into a developed built-up area.

The study suggested that an ANN-CA simulation model is one of the most appropriate and effective approaches for simulating complex types of LULC changes, and it can be used for other regions with a similar level of complexity. From the outcomes of the ANN-CA simulation, barren and urban lands will expand by many folds in commercial, industrial, and residential areas over the next decades up to 2050. The outcomes of this study on LULC changes and its future prediction might be useful for regional policymakers and authorities in developing sustainable urban planning and improving living standards.

**Author Contributions:** Conceptualization, M.R.U.M.; data curation, M.T.Z. and M.F.B.; formal analysis, M.T.Z. and M.R.U.M.; funding acquisition, M.R.U.M.; investigation, M.T.Z. and M.R.U.M.; methodology, M.T.Z. and M.F.B.; project administration, M.R.U.M.; resources, M.R.U.M.; supervision, M.R.U.M.; validation, M.T.Z.; writing—original draft, M.T.Z.; writing—review and editing, M.R.U.M. All authors have read and agreed to the published version of the manuscript.

**Funding:** This research was funded by YUTP research project (cost center; 015LC0-044).

**Institutional Review Board Statement:** Not applicable.



**Informed Consent Statement:** Not applicable.

**Data Availability Statement:** Further information on data presented in this work can be obtained from the authors.

**Acknowledgments:** The authors would like to gratefully acknowledge the financial support provided under the YUTP grant (cost center; 015LC0-044). The first author would like to acknowledge Universiti Teknologi PETRONAS for providing support under Graduate Assistantship scheme. Free data availability of Landsat images at the website of United States Geological Survey (USGS) Department is also greatly acknowledged.

**Conflicts of Interest:** The authors declare no conflict of interest.

## References

1. Singh, A. Review Article Digital change detection techniques using remotely-sensed data. *Int. J. Remote. Sens.* **1989**, *10*, 989–1003. [[CrossRef](#)]
2. Houghton, R.A. The worldwide extent of land-use change. *Bioscience* **1994**, *44*, 305–313. [[CrossRef](#)]
3. Hathout, S. The use of GIS for monitoring and predicting urban growth in East and West St Paul, Winnipeg, Manitoba, Canada. *J. Environ. Manag.* **2002**, *66*, 229–238. [[CrossRef](#)]
4. Fei, L.; Shuwen, Z.; Jiuchun, Y.; Liping, C.; Haijuan, Y.; Kun, B. Effects of land use change on ecosystem services value in West Jilin since the reform and opening of China. *Ecosyst. Serv.* **2018**, *31*, 12–20. [[CrossRef](#)]
5. Guzha, A.; Rufino, M.C. Impacts of land use and land cover change on surface runoff, discharge and low flows: Evidence from East Africa. *J. Hydrol. Reg. Stud.* **2018**, *15*, 49–67. [[CrossRef](#)]
6. López, E.; Bocco, G.; Mendoza, M.; Duhau, E. Predicting land-cover and land-use change in the urban fringe: A case in Morelia city, Mexico. *Landsc. Urban Plan.* **2001**, *55*, 271–285. [[CrossRef](#)]
7. Jat, M.K.; Garg, P.; Khare, D. Monitoring and modelling of urban sprawl using remote sensing and GIS techniques. *Int. J. Appl. Earth Obs. Geoinf.* **2008**, *10*, 26–43. [[CrossRef](#)]
8. Guerra, F.; Puig, H.; Chaume, R. The forest-savanna dynamics from multi-date Landsat-TM data in Sierra Parima, Venezuela. *Int. J. Remote. Sens.* **1998**, *19*, 2061–2075. [[CrossRef](#)]
9. Lu, D.; Mausel, P.; Brondizio, E.; Moran, E. Change detection techniques. *Int. J. Remote. Sensing* **2004**, *25*, 2365–2401. [[CrossRef](#)]
10. Roy, A.; Inamdar, A.B. Multi-temporal Land Use Land Cover (LULC) change analysis of a dry semi-arid river basin in western India following a robust multi-sensor satellite image calibration strategy. *Heliyon* **2019**, *5*, e01478. [[CrossRef](#)] [[PubMed](#)]
11. Helmer, E.H.; Brown, S.; Cohen, W.B. Mapping montane tropical forest successional stage and land use with multi-date Landsat imagery. *Int. J. Remote. Sens.* **2000**, *21*, 2163–2183. [[CrossRef](#)]
12. Hussain, M.; Chen, D.; Cheng, A.; Wei, H.; Stanley, D. Change detection from remotely sensed images: From pixel-based to object-based approaches. *ISPRS J. Photogramm. Remote. Sens.* **2013**, *80*, 91–106. [[CrossRef](#)]
13. Singh, Y.; Ferrazzoli, P.; Rahmoune, R. Flood monitoring using microwave passive remote sensing (AMSR-E) in part of the Brahmaputra basin, India. *Int. J. Remote. Sens.* **2013**, *34*, 4967–4985. [[CrossRef](#)]
14. Alexakis, D.D.; Agapiou, A.; Tzouvaras, M.; Themistocleous, K.; Neocleous, K.; Michaelides, S.; Hadjimitsis, D. Integrated use of GIS and remote sensing for monitoring landslides in transportation pavements: The case study of Paphos area in Cyprus. *Nat. Hazards* **2013**, *72*, 119–141. [[CrossRef](#)]
15. Yattoo, S.A.; Sahu, P.; Kalubarme, M.H.; Kansara, B.B. Monitoring land use changes and its future prospects using cellular automata simulation and artificial neural network for Ahmedabad city, India. *GeoJournal* **2020**, *85*, 1–22. [[CrossRef](#)]
16. Vibhute, A.D.; Gawali, B.W. Analysis and modeling of agricultural land use using remote sensing and geographic information system: A review. *Int. J. Eng. Res. Appl.* **2013**, *3*, 81–91.
17. Rahman, A.; Kumar, S.; Fazal, S.; Siddiqui, M.A. Assessment of land use/land cover change in the north-west district of Delhi using remote sensing and GIS techniques. *J. Indian Soc. Remote. Sens.* **2012**, *40*, 689–697. [[CrossRef](#)]
18. Attri, P.; Chaudhry, S.; Sharma, S. Remote sensing & GIS based approaches for LULC change detection—A review. *Int. J. Curr. Eng. Technol.* **2015**, *5*, 3126–3137.
19. Jiang, X.; Lu, D.; Moran, E.; Calvi, M.F.; Dutra, L.V.; Li, G. Examining impacts of the Belo Monte hydroelectric dam construction on land-cover changes using multitemporal Landsat imagery. *Appl. Geogr.* **2018**, *97*, 35–47. [[CrossRef](#)]
20. Hazarika, N.; Das, A.K.; Borah, S.B. Assessing land-use changes driven by river dynamics in chronically flood affected Upper Brahmaputra plains, India, using RS-GIS techniques. *Egypt. J. Remote Sens. Space Sci.* **2015**, *18*, 107–118. [[CrossRef](#)]
21. Lopez-Granados, E.; Mendoza, M.E.; Gonzalez, D.I. Linking geomorphologic knowledge, RS and GIS techniques for analyzing land cover and land use change: A multitemporal study in the Cointzio watershed, Mexico. *Rev. Ambiente Agua* **2013**, *8*, 18–37.
22. Lambin, E.F.; Geist, H.; Lepers, E. Dynamics of land-use and land-cover change in tropical regions. *Annu. Rev. Environ. Resour.* **2003**, *28*, 205–241. [[CrossRef](#)]
23. Serra, P.; Pons, X.; Sauri, D. Land-cover and land-use change in a Mediterranean landscape: A spatial analysis of driving forces integrating biophysical and human factors. *Appl. Geogr.* **2008**, *28*, 189–209. [[CrossRef](#)]

24. Chowdhury, M.; Hasan, M.E.; Al Mamun, M.M.A. Land use/land cover change assessment of Halda watershed using remote sensing and GIS. *Egypt. J. Remote. Sens. Space Sci.* **2018**, *23*, 63–75. [[CrossRef](#)]
25. Mohamed, M.A. Monitoring of temporal and spatial changes of land use and land cover in metropolitan regions through remote sensing and GIS. *Nat. Resour.* **2017**, *8*, 353–369. [[CrossRef](#)]
26. El Gammal, E.A.; Salem, S.M.; El Gammal, A.E.A. Change detection studies on the world's biggest artificial lake (Lake Nasser, Egypt). *Egypt. J. Remote Sens. Space Sci.* **2010**, *13*, 89–99. [[CrossRef](#)]
27. Akinyemi, F.O. Land change in the central Albertine rift: Insights from analysis and mapping of land use-land cover change in north-western Rwanda. *Appl. Geogr.* **2017**, *87*, 127–138. [[CrossRef](#)]
28. Cheruto, M.C.; Kauti, M.K.; Kisangau, P.D.; Kariuki, P. Assessment of land use and land cover change using gis and remote sensing techniques: A case study of Makueni County, Kenya. *J. Remote. Sens. GIS* **2016**, *05*, 1000175. [[CrossRef](#)]
29. Yusof, F.M.; Jamil, N.R.; Laew, N.I.C.; Aini, N.; Manaf, L.A. Land use change and soil loss risk assessment by using geographical information system (GIS): A case study of lower part of Perak River. *IOP Conf. Ser. Earth Environ. Sci.* **2016**, *37*, 12065. [[CrossRef](#)]
30. Noh, N.S.M.; Sidek, L.M.; Wayayok, A.; Abdullah, A.F.; Basri, H.; Farhan, S.A.; Sulaiman, T.; Ariffin, A.B. Erosion and sediment control best management practices in agricultural farms for effective reservoir sedimentation management at Cameron Highlands. *Int. J. Recent Technol. Eng.* **2019**, *8*, 6198–6205. [[CrossRef](#)]
31. Hanif, M.F.; ul Mustafa, M.R.; Hashim, A.M.; Yusof, K.W. Spatio-temporal change analysis of perak river basin using remote sensing and GIS. In Proceeding of the 2015 International Conference on Space Science and Communication, Lakawi, Malaysia, 10–12 August 2015.
32. Wang, C.; Lei, S.; Elmore, A.J.; Jia, D.; Mu, S. Integrating temporal evolution with cellular automata for simulating land cover change. *Remote. Sens.* **2019**, *11*, 301. [[CrossRef](#)]
33. Arsanjani, J.J. Characterizing, monitoring, and simulating land cover dynamics using GlobeLand30: A case study from 2000 to 2030. *J. Environ. Manag.* **2018**, *214*, 66–75. [[CrossRef](#)]
34. Brown, D.; Band, L.E.; Green, K.O.; Irwin, E.G.; Jain, A.; Lambin, E.F.; Pontius, R.G.; Seto, K.C.; Turner, B.L., II; Verburg, P.H. *Advancing Land Change Modeling: Opportunities and Research Requirements*; The National Research Council Press: Amsterdam, The Netherlands, 2013.
35. Jiang, X.; Lin, M.; Zhao, J. Woodland cover change assessment using decision trees, support vector machines and artificial neural networks classification algorithms. In Proceedings of the 2011 Fourth International Conference on Intelligent Computation Technology and Automation, Shenzhen, China, 28–29 March 2011.
36. Zhang, P.; Gong, M.; Su, L.; Liu, J.; Li, Z. Change detection based on deep feature representation and mapping transformation for multi-spatial-resolution remote sensing images. *ISPRS J. Photogramm. Remote Sens.* **2016**, *116*, 24–41. [[CrossRef](#)]
37. Sivakumar, V. Urban mapping and growth prediction using remote sensing and GIS techniques, Pune, India. *ISPRS Int. Arch. Photogramm. Remote. Sens. Spat. Inf. Sci.* **2014**, *XL-8*, 967–970. [[CrossRef](#)]
38. Sinha, S.; Sharma, L.K.; Nathawat, M.S. Improved land-use/land-cover classification of semi-arid deciduous forest land-scape using thermal remote sensing. *Egypt. J. Remote Sens. Space Sci.* **2015**, *18*, 217–233.
39. Subedi, P.; Subedi, K.; Thapa, B. Application of a hybrid cellular automaton—Markov (CA-Markov) model in land-use change prediction: A case study of Saddle Creek Drainage Basin, Florida. *Appl. Ecol. Environ. Sci.* **2013**, *1*, 126–132. [[CrossRef](#)]
40. Zhan, X.; Sohlberg, R.; Townshend, J.; DiMiceli, C.; Carroll, M.; Eastman, J.; Hansen, M.; DeFries, R. Detection of land cover changes using MODIS 250 m data. *Remote. Sens. Environ.* **2002**, *83*, 336–350. [[CrossRef](#)]
41. Zeng, Y.; Wu, G.; Zhan, F. Modeling spatial land use pattern using autologistic regression. *Int. Arch. Photogramm. Remote Sens. Spat. Inf. Sci.* **2008**, *37*, 115–119.
42. Schneider, L.C.; Pontius, R.G., Jr. Modeling land-use change in the Ipswich watershed, Massachusetts, USA. *Agric. Ecosyst. Environ.* **2001**, *85*, 83–94. [[CrossRef](#)]
43. Harun, N.; Yaacob, W.Z.W.; Simon, N. Potential areas for the near surface disposal of radioactive waste in Pahang. *AIP Conf. Proc.* **2016**, *1784*, 060021. [[CrossRef](#)]
44. Omar, M.N.; Rahaman, Z.A.; Hashim, M. the development of a soil erosion risk map for Perak, Malaysia. *Int. J. Acad. Res. Bus. Soc. Sci.* **2018**, *8*, 1108–1123. [[CrossRef](#)]
45. USGS. United States Geological Survey. Available online: [https://www.usgs.gov/faqs/what-are-band-designations-landsat-satellites?qt-news\\_science\\_products=0#qt-news\\_science\\_products](https://www.usgs.gov/faqs/what-are-band-designations-landsat-satellites?qt-news_science_products=0#qt-news_science_products) (accessed on 27 February 2021).
46. Sun, Y.; Ren, H.; Zhang, T.; Zhang, C.; Qin, Q. Crop leaf area index retrieval based on inverted difference vegetation index and NDVI. *IEEE Geosci. Remote. Sens. Lett.* **2018**, *15*, 1662–1666. [[CrossRef](#)]
47. McFeeters, S.K. Using the normalized difference water index (NDWI) within a geographic information system to detect swimming pools for mosquito abatement: A practical approach. *Remote. Sens.* **2013**, *5*, 3544–3561. [[CrossRef](#)]
48. Li, W.; Du, Z.; Ling, F.; Zhou, D.; Wang, H.; Gui, Y.; Sun, B.; Zhang, X. A comparison of land surface water mapping using the normalized difference water index from TM, ETM+ and ALI. *Remote. Sens.* **2013**, *5*, 5530–5549. [[CrossRef](#)]
49. Delbart, N.; Kergoat, L.; Le Toan, T.; Lhermitte, J.; Picard, G. Determination of phenological dates in boreal regions using normalized difference water index. *Remote. Sens. Environ.* **2005**, *97*, 26–38. [[CrossRef](#)]
50. Mas, J.F. Monitoring land-cover changes: A comparison of change detection techniques. *Int. J. Remote. Sens.* **1999**, *20*, 139–152. [[CrossRef](#)]

51. Karakuş, C.B. The Impact of Land Use/Land Cover (LULC) changes on land surface temperature in sivas city center and its surroundings and assessment of urban heat island. *Asia-Pac. J. Atmos. Sci.* **2019**, *55*, 669–684. [CrossRef]
52. Ibrahim, F.U.; Rasul, G. Urban land use land cover changes and their effect on land surface temperature: Case study using Dohuk City in the Kurdistan Region of Iraq. *Climate* **2017**, *5*, 13. [CrossRef]
53. Gao, J.; Liu, Y. Determination of land degradation causes in Tongyu County, Northeast China via land cover change detection. *Int. J. Appl. Earth Obs. Geoinf.* **2010**, *12*, 9–16. [CrossRef]
54. Bolstad, P.T.M. Rapid maximum likelihood classification. *Photogramm. Eng. Remote Sens.* **1991**, *57*, 67–74.
55. El-Tantawi, A.M.; Bao, A.; Chang, C.; Liu, Y. Monitoring and predicting land use/cover changes in the Aksu-Tarim River Basin, Xinjiang-China (1990–2030). *Environ. Monit. Assess.* **2019**, *191*, 480. [CrossRef]
56. Tallón-Ballesteros, A.J.; Riquelme, J.C. Data mining methods applied to a digital forensics task for supervised machine learning. In *Computational Intelligence in Digital Forensics: Forensic Investigation and Applications*; Springer: Berlin/Heidelberg, Germany, 2014; Chapter 17; pp. 413–428.
57. Zhang, J.; Goodchild, M.F. *Uncertainty in Geographical Information*; CRC Press: Boca Raton, FL, USA, 2002.
58. Kumar, M.; Mondal, I.; Pham, Q.B. Monitoring forest landcover changes in the Eastern Sundarban of Bangladesh from 1989 to 2019. *Acta Geophys.* **2021**, *69*, 561–577. [CrossRef]
59. Han, H.; Yang, C.; Song, J. Scenario simulation and the prediction of land use and land cover change in Beijing, China. *Sustainability* **2015**, *7*, 4260–4279. [CrossRef]
60. MOLUSCE. Modules for Land Use Change Evaluation. Available online: [https://wiki.gis-lab.info/w/Landscape\\_change\\_analysis\\_with\\_MOLUSCE\\_-\\_methods\\_and\\_algorithms](https://wiki.gis-lab.info/w/Landscape_change_analysis_with_MOLUSCE_-_methods_and_algorithms) (accessed on 21 March 2021).
61. Al-Rubkhi, M.N.A.G. Land Use Change Analysis and Modeling Using Open Source (QGis)-Case Study: Boasher Willayat. Ph.D. Thesis, College of Arts and Social Science, Department of Geography, Sultan Qaboos University, Muscat, Oman, 2017.
62. Gasarovic, M.; Jogun, T. The effect of fusing Sentinel-2 bands on land-cover classification. *Int. J. Remote Sens.* **2018**, *39*, 822–841. [CrossRef]
63. Pijanowski, B.C.; Brown, D.; A Shellito, B.; A Manik, G. Using neural networks and GIS to forecast land use changes: A Land Transformation Model. *Comput. Environ. Urban Syst.* **2002**, *26*, 553–575. [CrossRef]
64. Rumelhart, D.; Hinton, G.; Williams, R. *Learning Internal Representations by Error Propagation*; California University of San Diego, La Jolla Institute for Cognitive Science: San Diego, CA, USA, 1985.
65. Lau, K.H.; Kam, B.H. A cellular automata model for urban land-use simulation. *Environ. Plan. B Plan. Des.* **2005**, *32*, 247–263. [CrossRef]
66. Lantman, J.v.S.; Verburg, P.H.; Bregt, A.; Geertman, S. Core principles and concepts in land-use modelling: A literature review. In *Land-Use Modelling in Planning Practice*; Koomen, E., Borsboom-van, B.J., Eds.; Springer: Dordrecht, The Netherlands, 2011; pp. 35–57. [CrossRef]
67. Jogun, T.; Lukić, A.; Gašparović, M. Simulation model of land cover changes in a post-socialist peripheral rural area: Pozga-Slavonia County, Croatia. *Croat. Geogr. Bull.* **2019**, *81*, 31–59. [CrossRef]
68. GIS-Lab. Landscape Change Analysis with Methods of Land Use Change Evaluation (MOLUSCE) Methods and Algorithms 2018. Available online: [https://wiki.gislab.info/w/Landscape\\_change\\_analysis\\_with\\_MOLUSCE\\_methods\\_and\\_algorithms](https://wiki.gislab.info/w/Landscape_change_analysis_with_MOLUSCE_methods_and_algorithms) (accessed on 8 March 2021).
69. Pontius, R.G.; Huffaker, D.; Denman, K. Useful techniques of validation for spatially explicit land-change models. *Ecol. Model.* **2004**, *179*, 445–461. [CrossRef]
70. Wright, J.; Lillesand, T.M.; Kiefer, R.W. Remote sensing and image interpretation. *Geogr. J.* **1980**, *146*, 448. [CrossRef]
71. Jakovljevic, G.; Govedarica, M.; Álvarez-Taboada, F. Waterbody mapping: A comparison of remotely sensed and GIS open data sources. *Int. J. Remote Sens.* **2018**, *40*, 2936–2964. [CrossRef]
72. Ali, T.; Shahbaz, B.; Suleri, A. Analysis of myths and realities of deforestation in Northwest Pakistan: Implications for forestry extension. *Int. J. Agric. Biol.* **2006**, *8*, 107–110.
73. Butt, A.; Shabbir, R.; Ahmad, S.S.; Aziz, N. Land use change mapping and analysis using remote sensing and GIS: A case study of Simly watershed, Islamabad, Pakistan. *Egypt. J. Remote Sens. Space Sci.* **2015**, *18*, 251–259.
74. Pakistan, I.U.C.N. *Rapid Environmental Appraisal of Developments in and Around Murree Hills*; Technical Report; IUCN: Karachi, Pakistan, 2005.
75. Gong, P.; Li, X.; Zhang, W. 40-Year (1978–2017) human settlement changes in China reflected by impervious surfaces from satellite remote sensing. *Sci. Bull.* **2019**, *64*, 756–763. [CrossRef]
76. Al-Faraj, F.A.; Scholz, M. Impact of upstream anthropogenic river regulation on downstream water availability in transboundary river watersheds. *Int. J. Water Resour. Dev.* **2014**, *31*, 28–49. [CrossRef]
77. Drieschova, A.; Giordano, M.; Fischhendler, I. Governance mechanisms to address flow variability in water treaties. *Glob. Environ. Chang.* **2008**, *18*, 285–295. [CrossRef]
78. Veldkamp, T.; Wada, Y.; Aerts, J.; Döll, P.; Gosling, S.N.; Liu, J.; Masaki, Y.; Oki, T.; Ostberg, S.; Pokhrel, Y.; et al. Water scarcity hotspots travel downstream due to human interventions in the 20th and 21st century. *Nat. Commun.* **2017**, *8*, 15697. [CrossRef]
79. Villarini, G.; Smith, J.A.; Baeck, M.L.; Sturdevant-Rees, P.; Krajewski, W.F. Radar analyses of extreme rainfall and flooding in urban drainage basins. *J. Hydrol.* **2010**, *381*, 266–286. [CrossRef]
80. Bronstert, A. Floods and climate change: Interactions and impacts. *Risk Anal.* **2003**, *23*, 545–557. [CrossRef]

- 
81. Saputra, M.H.; Lee, H.S. Prediction of land use and land cover changes for North Sumatra, Indonesia, using an artificial-neural-network-based cellular automaton. *Sustainability* **2019**, *11*, 3024. [[CrossRef](#)]
  82. Memarian, H.; Balasundram, S.K.; Bin Talib, J.; Sung, C.T.B.; Sood, A.M.; Abbaspour, K. Validation of CA-Markov for Simulation of land use and cover change in the Langat Basin, Malaysia. *J. Geogr. Inf. Syst.* **2012**, *04*, 542–554. [[CrossRef](#)]